Predictions of Stepped Isotherms in Breathing Adsorbents by the Rigid Adsorbent Lattice Fluid

Predictions of Stepped Isotherms in Breathing Adsorbents by the Rigid Adsorbent Lattice Fluid

Maarten C. Verbraeken* and Stefano Brandani

School of Engineering, University of Edinburgh, The King's Buildings, Robert Stevenson Road, EH9 3FB

*mverbrae@ed.ac.uk

Abstract

Adsorbents that undergo structural changes in the presence of adsorbate molecules are an interesting new class of materials, which could offer enhanced selectivity, purity and recovery in separation technology. To date however, their application in such technology is hampered by the lack of a simple, consistent thermodynamic framework, which can effectively describe and predict their adsorption behaviour under a range of conditions. This becomes especially true for their behaviour in multicomponent adsorbate mixtures, for which experimental data is limited and cumbersome to obtain. Here we present how the relatively simple Rigid Adsorbent Lattice Fluid model successfully and accurately predicts stepped isotherms in the breathing MOF, MIL-53 (Al) in the presence of CO_2 and CH_4. Breathing transitions are predicted solely on the basis of the different densities of the material's two structural configurations and their associated Gibbs energies. Hysteresis effects can easily be included by considering the structures' osmotic stress, which can be calculated readily from the lattice fluid expressions. The model can be parameterised with a minimum of experimental or simulated data, subsequently becoming predictive, and since the model has its origins in statistical mechanics, no prior assumptions, such as Langmuir type behaviour are required, presenting a major advantage over existing (semi)-empirical models. The approach shown in this study should furthermore be generic and should equally well apply to other flexible adsorbents.

Introduction

Separation processes typically make up 40 – 90 % of a chemical plant's capital cost, so their importance can hardly be overstated. Separation by adsorption is versatile, robust and highly scalable and its use is therefore commonplace. Adsorption is particularly promising for selectively capturing carbon dioxide, for instance from effluent streams in power plants and industrial processes but also directly from air, and may thus be a key technology in mitigating climate change. Many adsorbents exhibit some level of flexibility upon adsorbing guest molecules and indeed this has become the focus of much research in recent years[1–4]. Metal organic frameworks (MOFs) are an obvious example of such flexibility, since their organic linkers provide them with varying degrees of configurational freedom. This may manifest itself simply in contraction/expansion upon adsorption, but more unusual behaviour, such as gate-opening and breathing has also been widely reported[5]. Structural changes are not exclusively induced by adsorption, but may be triggered by temperature and mechanical pressure, for instance. Even adsorbents that traditionally are considered rigid, such as zeolites, often show a limited degree of structural flexibility and this can be used effectively to tailor adsorptive behaviour and selectivity[1,3,6]. Gating effects for instance, allow only certain molecules to enter a solid's micropores[3,7], whereas structural breathing could provide a large working capacity over a small pressure range in pressure swing adsorption processes[8,9]. Due to their high degree of customisability, flexible adsorbent are evidently highly sought after as next generation materials in adsorptive processes. Their successful application into real-life industrial processes however, is as of yet not straightforward, as the flexibility can have unpredictable effects on critical process parameters, such as recovery and purity. This is because the effective design and optimisation of these processes requires a thorough understanding of the system's thermodynamics, but including the materials' flexibility in such a thermodynamic description has proved very challenging to date.

Traditional thermodynamic models, such as those based on Gibbs isotherms or the Ideal Adsorbed Solution Theory (IAST), are powerful tools, but are derived on the assumption that the adsorbent material is inert, with the consequence that any terms relating to the adsorbent drop out of the equations[10,11]. It is clear however, that the adsorbent's flexibility is a direct result from the interaction with the guest molecules and hence a full thermodynamic description of such an adsorption system should include the thermodynamic properties of the solid material as well as the adsorbate molecules. Alternative models that introduce adsorbate-adsorbate and adsorbate-adsorbent interactions to describe non-idealities have indeed been developed, but these still do not account for a changing solid[10]. As it is fiendishly difficult to retrofit the adsorbent's flexibility into existing thermodynamic models, most research in this area resort to molecular simulations to reproduce and predict isotherms. Although this method is generally very successful and, in the appropriate ensemble, can provide valuable insights from molecular to macroscopic scales[12–16], the obvious drawback is the computational demand, which is prohibitive in process simulation. A semi-empirical approach was

instead pursued by Coudert and co-workers for the particular case of breathing MOFs and related structural transitions, by developing a thermodynamic model, which determines phase stability in the osmotic ensemble[2,17]. The model was further developed by Neimark et al. to include osmotic stress as a means to explain hysteresis effects[18]. Despite describing experimental results accurately and being generic, the model requires many fitting parameters and is rather reliant on experimental data and is therefore not entirely predictive. Dunne and Manos developed a quasi-one dimensional statistical mechanical model in the osmotic ensemble, which conceptually describes breathing and requires little computing power[19,20]. Simon et al. also developed a one-dimensional model to describe the effect of rotating ligands in MOFs on isotherms and further expanded the model using a mean field approximation[21]. It is clear that the pursuit of a thermodynamic model which can both accurately predict the adsorption behaviour of flexible materials with few modelling parameters and which is computationally light would be highly relevant in designing and optimising separation processes.

Here we propose to build such a model by using a lattice fluid (LF) model, specifically developed for crystalline solid adsorbents. The LF is a concept which was initially developed by Sanchez and Lacombe to describe the thermodynamics of polymers, but since it is essentially an equation of state, it can apply equally well to any fluid or solid component[22–24]. Danner and co-workers have shown that an LF based approach can be used to describe adsorption on solids, whilst allowing for non-idealities[25,26]. LF models lead to relatively simple expressions for the Gibbs free energy of the system and hence, through differentiation with respect to the component number of moles/molecules, N_i, the chemical potentials of these components. This approach has previously been used by Doghieri and Sarti with co-workers to successfully predict adsorption behaviour in glassy polymers[27–29]. The main purpose of their non-equilibrium lattice fluid (NELF) was to generate isotherms however, which does not require any thermodynamic expressions for the adsorbent. In addition, the expressions for the Gibbs energy in previous versions of the LF model are neither excess nor residual energies, which leads to issues at low partial pressures. To address these two issues, Brandani introduced the Rigid Adsorbent Lattice Fluid (RALF) model, which was shown to describe the adsorption behaviour of various molecules on silicalite with good accuracy, i.e. better than the empirical Toth model[30]. The model is additionally well suited for describing multicomponent adsorption systems from pure component isotherms, making it a powerful predictive tool, despite its relative simplicity.

Whereas the work by Brandani assumed the solid to be in the *frozen* limit, i.e. not undergoing dimensional changes upon adsorption, in this paper we are extending the RALF model to describe the adsorption behaviour of a flexible material. The focus will be on MIL-53 (Al), a breathing MOF, which has been described in great detail in recent literature[16,31–39]. This material exhibits dramatic volume changes of approximately 40% between a large pore (*lp*) and narrow pore (*np*) structure. A number of studies have attempted to model this behaviour, from the semi-empirical work by the

groups of Boutin, Fuchs and Neimark[2,18,33] to full thermodynamic descriptions through molecular simulations[12,15,37,40–42]. We will show that, using just the density of the solid material and a small number of fitting parameters, the relatively simple RALF model can capture the effect of breathing on the experimentally observed isotherms. Although we focus on this particular material, the approach we use is generic and should apply to any combination of guest molecule/adsorbent.

Theory

The Rigid Adsorbent Lattice Fluid and its equations have been described in great detail in ref. [30]. The equations can also be found in the supporting information, Appendix 1. In essence, the RALF model represents an equation of state with a corresponding expression for the Gibbs energy for the solid phase. Even though the RALF model is perfectly suited to deal with multicomponent systems, here we opt for a single adsorbate model to describe the breathing behaviour of MIL-53 (Al). For such a system, the residual Gibbs energy is given by:

$$\frac{G^R(T,P,N)}{RT} = rN\left[-\frac{\tilde{\rho}}{\tilde{T}} + \frac{(1-\tilde{\rho})\ln(1-\tilde{\rho})}{\tilde{\rho}} + 1\right] + N(z - 1 - \ln z) \quad (1)$$

Here we opt for the chemical engineering nomenclature as used in various textbooks, where the term residual refers to the departure of a thermodynamic property from that of an ideal gas at the same temperature and pressure[43,44] .

Equation. 1 is the expression for the residual Gibbs energy of the adsorbed phase given in ref.[30] written for a single adsorbate, given that the combinatorial term for a single adsorbate becomes zero due to the rigid nature of the solid. The reduced quantities are defined by:

$$\tilde{T} = \frac{T}{T^*} \qquad \tilde{P} = \frac{P}{P^*} \qquad \tilde{\rho} = \frac{\rho}{\rho^*}$$

The compressibility factor is as usual, i.e. $z = \frac{PV}{NRT} = r\frac{\tilde{P}}{\tilde{\rho}\tilde{T}}$. For an adsorbent, the density of the mixture does not correspond to the equilibrium value as given by an Equation of State. For the compressibility factor of a single component in equilibrium, z^{EoS}, the following holds:

$$z^{EoS} - 1 = r\left[-\frac{\tilde{\rho}}{\tilde{T}} - \frac{\ln(1-\tilde{\rho})}{\tilde{\rho}} - 1\right] \quad (2)$$

As is evident from equation 1, knowledge of the density of the system is essential to obtain the Gibbs energy and the chemical potentials in RALF. The volume of the adsorbent including the micropores, V_s, is taken as the system volume and therefore the density is given by:

$$\rho = \frac{\sum_j m_j}{V_s} = \frac{m_s}{w_s V_s} = \frac{\rho_s}{w_s} \quad (3)$$

where w_s is the weight fraction of the solid.

A generic formula for V_s was proposed by Brandani:

$$V_s = V_s^{\infty} + (V_s^0 - V_s^{\infty}) e^{-\beta_T P} + \Delta V_s \quad (4)$$

Where V_s^{∞} and V_s^0 are the volumes at infinite pressure and in vacuum, respectively. β_T is the isothermal compressibility and the final term describes the volume changes due to adsorption. The compressibility term is expected to be negligible under typical conditions for adsorption systems, and thus

$$V_s = V_s^0 + \Delta V_s \quad (5)$$

The term ΔV_s can be determined from *in situ* diffraction experiments under adsorption conditions, or, if such data is not available, it can be used as an adjustable term to allow the model to accurately describe experimental data.

For the calculation of adsorption isotherms, we need an equilibrium condition. The condition is for the chemical potentials of component *j* to be equal in the adsorbed and fluid phase. The subscript *A* is added for clarity in equation 6 to describe the adsorbed phase, but will be dropped from now on. Isotherms can be constructed by solving equation 6 for the number of moles adsorbed at any given combination of pressure and temperature.

$$\mu_{k,F}(P,T) = \mu_{k,A}(N_k, P, T) \quad (6)$$

In the RALF model the chemical potential of the adsorbed phase is expressed on a molar basis, whereas that of the solid phase is expressed on a mass basis.

$$\frac{{\mu_k}^R}{RT} = \frac{1}{RT}\left(\frac{\partial G^R}{\partial N_k}\right)_{T,P,N_{j\neq k}} = \ln\varphi_k$$

$$\frac{{\mu_s}^{Rm}}{RT} = \frac{1}{RT}\left(\frac{\partial G^R}{\partial m_s}\right)_{T,P,N_{j\neq s}}$$

Since these are residual chemical potentials, $\frac{{\mu_k}^R}{RT}$ directly yields the logarithm of the fugacity coefficient for component *k*, φ_k.

Chemical potentials

The chemical potential for a single adsorbate component is given by equation 7. The derivations for the chemical potentials can be found in the Appendix.

$$\frac{{\boldsymbol{\mu_1}}^{\boldsymbol{R}}}{\boldsymbol{RT}} = -\frac{\tilde{\boldsymbol{\rho}}}{\tilde{\boldsymbol{T}}}\left(\frac{\mathbf{2}\sum_j \boldsymbol{\phi_j P^*_{j1}}}{\boldsymbol{P^*}} - \mathbf{1}\right)\boldsymbol{r_1} + \left[\frac{(\mathbf{1}-\tilde{\boldsymbol{\rho}})\mathbf{ln}(\mathbf{1}-\tilde{\boldsymbol{\rho}})}{\tilde{\boldsymbol{\rho}}} + \mathbf{1}\right]\boldsymbol{r_1^0} + \left(\mathbf{1} + \frac{\boldsymbol{rN}}{\boldsymbol{r_1\rho_s}}\frac{\boldsymbol{\partial\rho_s}}{\boldsymbol{\partial N_1}}\right)\left(\boldsymbol{z^{EoS}} - \mathbf{1}\right)\frac{\boldsymbol{r_1}}{\boldsymbol{r}} - \mathbf{ln}\boldsymbol{z} - \frac{\boldsymbol{z}-\mathbf{1}}{\boldsymbol{r}}\frac{\boldsymbol{rN}}{\boldsymbol{\rho_s}}\frac{\boldsymbol{\partial\rho_s}}{\boldsymbol{\partial N_1}} \quad (7)$$

Where z^{EoS} has been defined previously (equation 2). In comparison with the equivalent expression given for the *frozen* solid in ref. [30], the expression in equation 7 now includes two terms to reflect the volumetric changes in the solid, namely.

$$\frac{{\boldsymbol{\mu_1}}^{\boldsymbol{R,flexible}}}{\boldsymbol{RT}} - \frac{{\boldsymbol{\mu_1}}^{\boldsymbol{R,frozen}}}{\boldsymbol{RT}} = \frac{\boldsymbol{rN}}{\boldsymbol{r_1\rho_s}}\frac{\boldsymbol{\partial\rho_s}}{\boldsymbol{\partial N_1}}\left(\boldsymbol{z^{EoS}} - \mathbf{1}\right)\frac{\boldsymbol{r_1}}{\boldsymbol{r}} - \frac{\boldsymbol{z}-\mathbf{1}}{\boldsymbol{r}}\frac{\boldsymbol{rN}}{\boldsymbol{\rho_s}}\frac{\boldsymbol{\partial\rho_s}}{\boldsymbol{\partial N_1}} \quad (8)$$

The corresponding chemical potential for the ideal gas is:

$$\frac{{\mu_1}^{IG}}{RT} = \frac{{\mu_1}^{IG}(P^0,T)}{RT} + \ln\frac{P}{P^0} \quad (9)$$

The chemical potential for the fluid phase is given by:

$$\frac{{\boldsymbol{\mu_{1,F}}}^{\boldsymbol{R}}}{\boldsymbol{RT}} = \left[-\frac{\tilde{\boldsymbol{\rho}}_\mathbf{1}}{\tilde{\boldsymbol{T}}_\mathbf{1}} + \frac{(\mathbf{1}-\tilde{\boldsymbol{\rho}}_\mathbf{1})\mathbf{ln}(\mathbf{1}-\tilde{\boldsymbol{\rho}}_\mathbf{1})}{\tilde{\boldsymbol{\rho}}_\mathbf{1}} + \mathbf{1}\right]\boldsymbol{r_1^0} + \boldsymbol{z} - \mathbf{1} - \mathbf{ln}\boldsymbol{z} \quad (10)$$

Where $\tilde{\rho}_1$ is the reduced density of the single component in the fluid according to the equation of state, which is calculated by solving:

$$r_1^0 \frac{\widetilde{P}_1}{\widetilde{T}_1} = \left[-\frac{\widetilde{\rho}_1{}^2}{\widetilde{T}_1} - \widetilde{\rho}_1 - -\ln(1-\widetilde{\rho}_1) \right] r_1^0 + \widetilde{\rho}_1 \qquad (11)$$

The chemical potential for the solid is given by:

$$\frac{\mu_s{}^{Rm}}{RT} = -\frac{\widetilde{\rho}}{\widetilde{T}} \frac{rN\phi_s}{m_s} \left(\frac{2\sum_j \phi_j P_{js}^*}{P^*} - 1 \right) + \frac{\widetilde{\rho}\phi_s}{\rho_s v_s^*} \left[\frac{(1-\widetilde{\rho})\ln(1-\widetilde{\rho})}{\widetilde{\rho}} + 1 \right] + \frac{N}{m_s} \left(\phi_s - 1 + \frac{m_s}{\rho_s} \frac{\partial \rho_s}{\partial m_s} \right) \left(z^{EoS} - 1 \right) + \frac{N}{m_s} (z-1) \left(1 - \frac{m_s}{\rho_s} \frac{\partial \rho_s}{\partial m_s} \right) - \frac{N_s}{m_s} \ln z \qquad (12)$$

And for the pure solid at system pressure *P* (i.e. with no adsorbates):

$$\frac{\mu_{s,0}{}^{Rm}}{RT} = \frac{1}{\rho_s^* v_s^*} \left[\frac{(1-\widetilde{\rho})\ln(1-\widetilde{\rho})}{\widetilde{\rho}} + 1 - \frac{\widetilde{\rho}_s}{\widetilde{T}_s} + \frac{m_s}{r_s^0 \rho_s} \frac{\partial \rho_s}{\partial m_s} \left(z^{EoS} - 1 \right) \right] + \frac{P}{RT\rho_s} \left(1 - \frac{m_s}{\rho_s} \frac{\partial \rho_s}{\partial m_s} \right) \qquad (13)$$

The additional terms as compared to the expression for the *frozen* solid are:

$$\frac{\mu_s{}^{Rm,flexible}}{RT} - \frac{\mu_s{}^{Rm,frozen}}{RT} = \frac{N}{m_s} \left(\frac{m_s}{\rho_s} \frac{\partial \rho_s}{\partial m_s} \right) \left(z^{EoS} - 1 \right) - \frac{N}{m_s} (z-1) \left(\frac{m_s}{\rho_s} \frac{\partial \rho_s}{\partial m_s} \right) \qquad (14)$$

$$\frac{\mu_{s,0}{}^{Rm,flexible}}{RT} - \frac{\mu_{s,0}{}^{Rm,frozen}}{RT} = \frac{1}{\rho_s^* v_s^*} \left[\frac{m_s}{r_s^0 \rho_s} \frac{\partial \rho_s}{\partial m_s} \left(z^{EoS} - 1 \right) \right] - \frac{P}{RT\rho_s} \left(\frac{m_s}{\rho_s} \frac{\partial \rho_s}{\partial m_s} \right) \qquad (15)$$

Equation 13 allows for an internal consistency check of the RALF model, by allowing 2 distinct ways for calculating the reduced grand potential, Ψ. For a single component:

$$\Psi = \frac{\mu_s{}^{Rm} - \mu_{s,0}{}^{Rm}}{RT} = -\int_0^f n_1 \, d\ln f \qquad (16)$$

where n_1 is the adsorbed amount in moles per unit mass.

Parameterising adsorption on MIL-53 (Al)

In order for the lattice fluid model to accurately describe the thermodynamics of the adsorbate – adsorbent system under consideration, it requires pure component characteristic parameters as outlined in ref. [30]. Consequently, through a set of mixing rules, these pure component parameters yield the characteristic parameters for the solid phase (itself a mixture of $N_{ads}+1$ components in the case of N_{ads} adsorbates; $N_{ads}=1$ in this work) at varying composition. Here we opt to define the pure components by their close-packed density, ρ^*, energy density, P^* and interaction energy, T^*. For several molecules these parameters can be found in the literature or, when no such information is available, can alternatively be extracted from saturated vapour pressure data as suggested by Sanchez and Lacombe [22,45]. Table 1 lists a number of adsorbate molecules with their characteristic parameters.

Table 1: Characteristic parameters for Lattice Fluid EoS for various adsorbate molecules

Molecule	$\boldsymbol{P}^*$ (MPa)	$\boldsymbol{T}^*$ (K)	$\boldsymbol{\rho}^*$ (kg/m^3)	*M (kg/mol)*
CO	141	204	919	0.028
N_2	145	160	943	0.028
CH_4	215	250	500	0.016
C_2H_6	320	330	640	0.030
CO_2	300	630	1515	0.044
Xe	304	351	3360	0.131

Characteristic parameters for the solid

The adsorbent under consideration in this work is MIL-53 (Al). This material should serve as a good candidate material to evaluate the versatility of the RALF model with respect to flexible materials. It is composed of metal oxide octahedra, linked by organic moieties, in this case terephtalate ions[38,34,9]. The material and its breathing behaviour are most easily imagined through an analogy of a collapsing/expanding wine rack. Under the appropriate conditions, the material essentially collapses from an orthorhombic structure with large pores (*lp*), into a monoclinic one with reduced pore volume, denoted as narrow pore (*np*). Whereas this transition involves a large increase in solid density, no bonds are broken upon this configurational change. The transition is depicted in Figure 1. Due to the fact that the chemical coordination does not change on going from one configuration to the other, it is expected that the characteristic parameters also remain unchanged. In other words, one set of characteristic parameters should describe both solid phases, with the only difference being the solid density. This is equivalent to keeping the force field parameters constant in a molecular simulation.

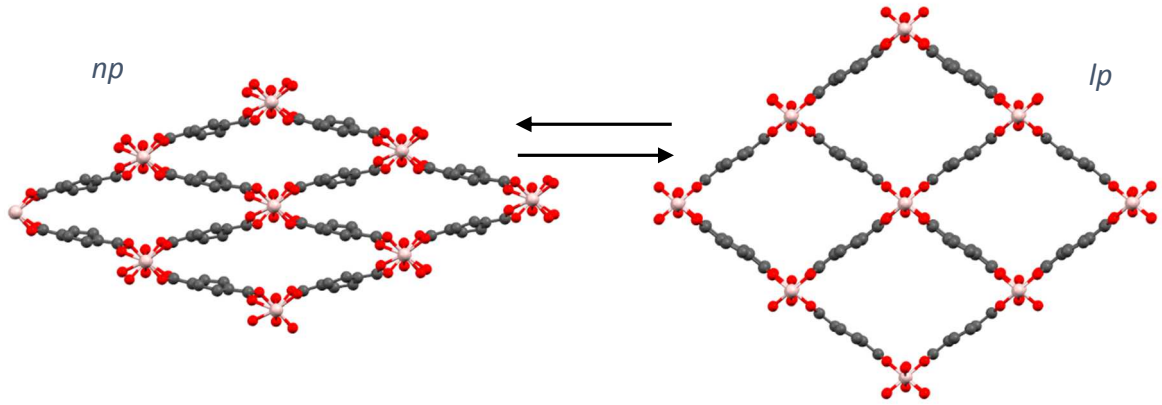

Figure 1: Structural transition in MIL-53 (Al) from narrow pore (np) to large pore (lp). Structure essentially opens up, like a wine rack, without creating or breaking chemical bonds. Structural information obtained from ref. [38]

Brandani suggested a suitable method to extract the pure component parameters for the solid, as no vapour pressure data is available for such phases[30]. The solid density ρ_s is based on the volume of the solid including the micropores and is directly obtained from crystallographic data. When the micropore volume is known, for instance through He-pycnometry, the close-packed density ρ_s^* can be obtained by:

$$\rho_s^* = \frac{\rho_s}{(1 - v_p)} \qquad (17)$$

where v_p is the pore volume fraction. Based on unit cell data for the *lp* structure under vacuum, $\rho_{s,lp} = 967$ kg m^{-3} at T = 295 K [31]. Literature values for v_p in the *lp* phase are approximately 0.54, giving $\rho_s^* = 2103$ kg m^{-3} [46,47].

The characteristic pressure, P_s^* can be obtained from adsorption energies or enthalpies at zero loading through[30]:

$$\Delta U_0 = \Delta H_0 - RT = \tilde{\rho}_s r_k^0 v_k^* 2 P_{ks}^* \qquad (18)$$

Adsorption energies for alkanes with differing carbon number are ideally suited for regression with P_s^* being the adjustable parameter. Here Monte Carlo simulation data for another breathing MOF, MIL-53 (Cr) is used, assuming the difference in adsorption energies between the two structures for both materials is similar[48]. Figure 2 shows how the adsorption energies for both structures can be fitted satisfactorily, assuming one common value for P_s^*. This confirms that the difference in adsorption enthalpies is due to the difference in densities only.

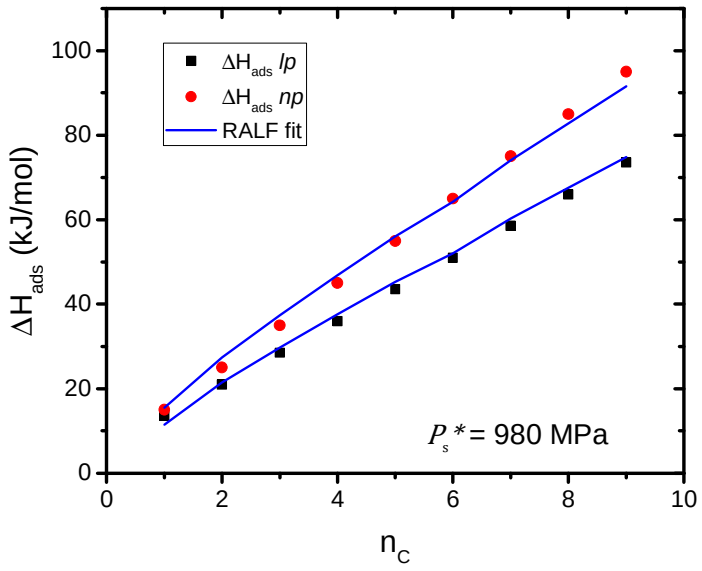

Figure 2: Regression of adsorption energy data from Monte Carlo simulations[48] for both np and lp structures. Both sets of data can be fitted using one value for $P_s^* = 980$ MPa, due to the different densities of the structures.

One final characteristic parameter is required to describe the solid in the LF model. With ρ_s^* and P_s^* in place, equation 21 can be used to determine v_s^* (and T_s^* through equation S10 in the supporting information) from experimental or simulated Henry law constants, K_P. Carrying this out for a number of molecules provides an initial estimate for T_s^*. Subsequent refinement can be achieved by full isotherm fitting. In order to obtain a reliable value for T_s^*, we have used isotherms of MIL-53 (Al) in the *lp* structure for cases where breathing is absent. We subsequently use the same T_s^* for both structures. Optimisation of the fits are additionally performed through adjusting values for the binary interaction parameter, κ_{ks}, and confinement parameter, ξ_{kA}, which are allowed to differ between the two structural configurations. These two parameters are defined by[30]:

$$v_{kA}^* = (1 + \xi_{kA})v_k^* \quad (19)$$

$$P_{ks}^* = P_{sk}^* = (1 - \kappa_{ks})\sqrt{P_s^* P_k^*} \quad (20)$$

Where v_k^* is the close packed volume of a lattice site, occupied by molecule *k*.

Figure 3 shows the fits of RALF with experimental data from various laboratories using $T_s^* = 750$ K [33,35,47].

$$\ln K_P = \ln\frac{m_s}{\rho_s RT} + \frac{\tilde{\rho}_s}{RT} r_k^0 v_k^* 2P_{ks}^* - r_k^0\left[\frac{(1-\tilde{\rho}_s)\ln(1-\tilde{\rho}_s)}{\tilde{\rho}_s} + 1\right] - r_k^0 \frac{v_k^*}{v_s^*}\left[-\frac{\ln(1-\tilde{\rho}_s)}{\tilde{\rho}_s} - 1\right] \quad (21)$$

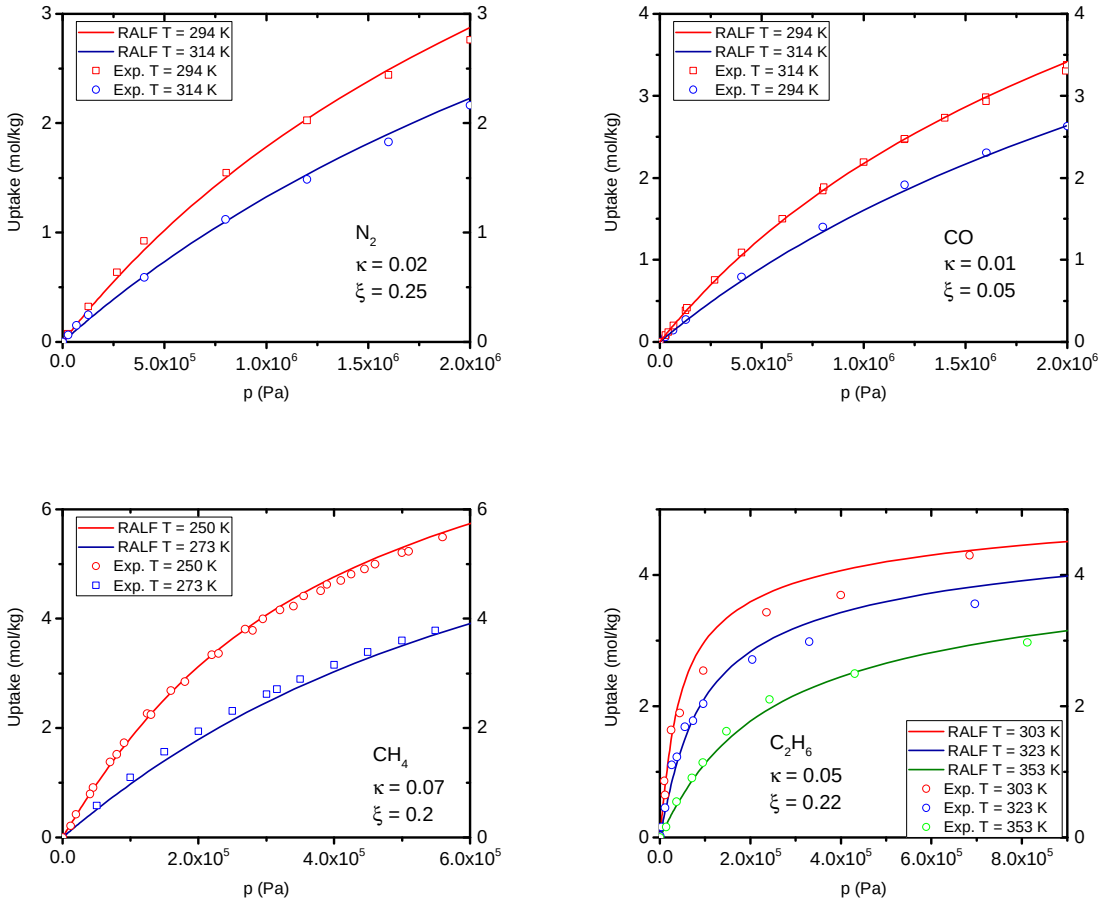

Figure 3: Experimental isotherms for various molecules in the lp structure of MIL-53 (Al)[33,35,47] *and RALF fits using* $T_s^* = 750\ K$.

Gibbs energy of the system and determining phase stability

The process of breathing involves a structural transition between the *lp* and *np* phases. In thermodynamic terms, this breathing transition must allow for a minimisation of the adsorbate – adsorbent system's free energy. In our system, we consider a system at constant pressure, temperature, mass of solid and number of moles of adsorbate molecules, described graphically in Figure 4. The system can be envisaged as containing a freely moving piston, which maintains the system pressure and thereby gas phase chemical potential upon adsorption or desorption. The solid can transition between its two configurations with corresponding chemical potentials, $\mu_{s,lp}$ and $\mu_{s,np}$. This transition involves exchanging adsorbate molecules with the gas phase. The Gibbs energy is the appropriate thermodynamic property to describe this system and the most stable configuration is the one with the lowest total Gibbs energy at any given conditions.

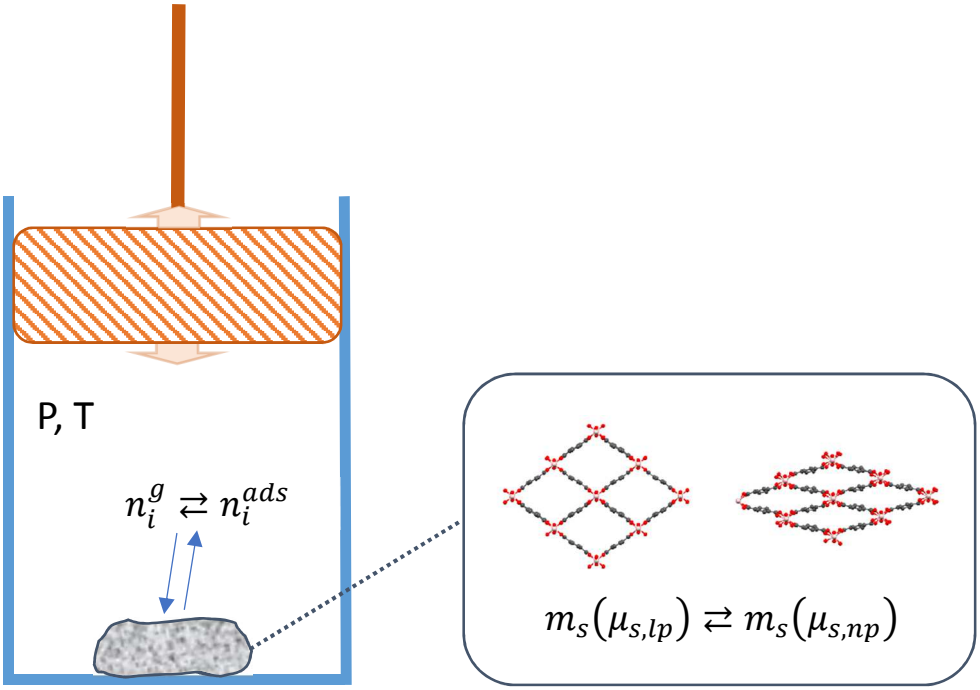

Figure 4: Schematic diagram of the adsorption system at constant pressure, temperature mass of solid and number of moles of adsorbate molecules. The solid can transition between two configurations, which involves exchanging molecules with the gas phase and a change in chemical potential for the solid itself. The piston can move freely and as such ensures constant pressure and hence constant chemical potential of the adsorbate molecules.

The Gibbs energy is given by:

$G = U + PV - TS$	22

And in differential form

$dG = VdP - SdT + \sum_k \mu_k dn_k$	23

Therefore at constant pressure and temperature:

$dG = \sum_k \mu_k dn_k = \sum_k {\mu_k}^g dn_k^g + \sum_k {\mu_k}^{ads} dn_k^{ads} + \mu_s dm_s$	24

Where the superscripts *g* and *ads* stand for gas phase and adsorbed phase, respectively. For an adsorption system in equilibrium, moles in the gas phase exchange with moles in the adsorbed phase, i.e.

$dn_k^g = -dn_k^{ads}$	25

And

$\mu_k^g = \mu_k^{ads}$	26

Additionally $dm_s = 0$ and therefore:

$dG = \sum_k \left(\mu_k{}^g - \mu_k{}^{ads}\right) dn_k^g = 0$	27

Which shows that the minimum in Gibbs energy is indeed the equilibrium condition. The total Gibbs energy is obtained by integrating equation 24:

$G^{Total} = \sum_k \mu_k{}^g n_k^g + \sum_k \mu_k{}^{ads} n_k^{ads} + \mu_s m_s = \sum_k \left(n_k^g + n_k^{ads}\right) \mu_k{}^g + \mu_s m_s$	28

Since at a given set of conditions the total number of adsorbate molecules, i.e. $n_k^g + n_k^{ads}$ is constant, as are m_s and μ_k^g, to determine the solid phase stability, one need only consider the chemical potential of the solid, μ_s.

This derivation is entirely equivalent to the use of the osmotic ensemble and osmotic potential to determine phase stability, as previously used in various studies[1,2,49]. These studies consider a system with two phases, one of which does not contain the solid component. By separating the fluid reservoir and solid phase using a semi-permeable wall, one can determine phase stability in the solid phase by considering its osmotic potential:

$\Omega_{OS} = U + PV - TS - \sum_k \mu_k{}^{ads} n_k^{ads} = G - \sum_k \mu_k{}^{ads} n_k^{ads}$	29

The two solid phases in refs[1,2,49] are considered rigid and the system is hence at constant volume and temperature. By invoking the grand canonical potential, Ω they show that:

$\Omega_{OS} = g_{s,0} + \int \left(\frac{\partial \Omega}{\partial \mu}\right)_{n,V} d\mu$	30

Where $g_s{}^0$ is the molar (or equivalent mass based) Gibbs energy for the solid at zero loading. For a single adsorbate component and using $\left(\frac{\partial \Omega}{\partial \mu}\right)_{n,V} = -n^{ads}$:

$\Omega_{OS} = g_{s,0} - \int_0^P n^{ads} d\mu^{ads} = g_{s,0} - RT \int_0^P n^{ads} d\ln f^{ads} = g_{s,0} + RT\Psi$ $= g_{s,0} + \left({\mu_s}^R - {\mu_{s,0}}^R\right)$	31

In the final equation, the integral can be recognised as the grand potential, as previously defined in equation 16. Finally recognising that $g_{s,0} = {g_{s,0}}^{ref} + {g_{s,0}}^R = {g_s}^{ref} + {\mu_{s,0}}^R$, equation 31 reduces to:

$\Omega_{OS} = {g_{s,0}}^{ref} + {\mu_s}^R = \mu_s$	32

Here we use ${g_{s,0}}^{ref}$ as a reference state instead of an ideal gas term, which is more appropriate for a solid. It is clear that determining phase stability through the osmotic potential is equivalent to finding the minimum in total Gibbs energy, i.e. equation 28.

As shown in the previous section the RALF model yields an explicit expression for the residual chemical potential for the solid and for the reduced grand potential. Rather than defining ${g_{s,0}}^{ref}$ for the solid phases, it is more straightforward to determine phase stability through the reduced grand potential in equation 31 and using $g_{s,0}$ as an adjustable parameter to the model. This parameter now effectively describes the Gibbs energy difference between the two phases at zero loading. If we choose to make the empty *lp* phase the reference state for the solid and introduce $\Delta g^0 = g_{np,0} - g_{lp,0}$, then:

$\frac{\Omega_{OS,lp}}{RT} = \frac{{\mu_{s,lp}}^{Rm} - {\mu_{s,lp,0}}^{Rm}}{RT} = \Psi_{lp}$	33
$\frac{\Omega_{OS,np}}{RT} = \frac{{\mu_{s,np}}^{Rm} - {\mu_{s,np,0}}^{Rm}}{RT} + \frac{\Delta g^0}{RT} = \Psi_{np} + \frac{\Delta g^0}{RT}$	34

Since $\Delta g^0 = \Delta h^0 - \mathrm{T}\Delta s^0$, we have the reference molar enthalpy and entropy differences of the empty structures as parameters to bring the solid's free energy in line with experimental observations and simulations. Both structures have been shown to have the same heat capacity, C_p and it is therefore reasonable to assume that Δh^0 and Δs^0 can be kept constant with temperature[50]. The relationship between reduced grand potential and reduced osmotic potential is shown schematically in Figure 5 and Figure 6. The structure with the lowest osmotic potential is thermodynamically the most stable configuration. The profile in Figure 6 therefore suggests that two structural transitions take place: *lp* $\rightarrow$ *np* at lower pressures and the reverse transition at higher pressures. The thus predicted structural transitions would correspond to the true equilibrium situations, i.e. it assumes the system can freely transition from one configuration to the other. In reality however, the free energy profile for the solid

– adsorbate system is likely to exhibit energy barriers, which will prevent the system from transitioning at the conditions as predicted by the osmotic potential.

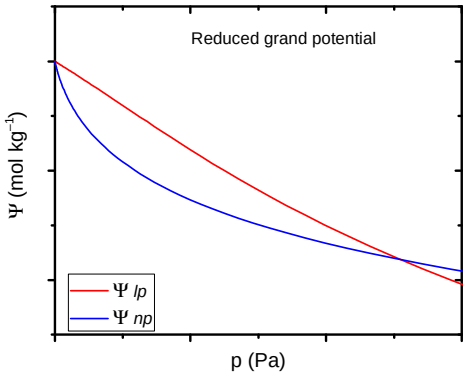

Figure 5: Schematic representation of reduced grand potential (Ψ) vs. pressure for both np and lp structures

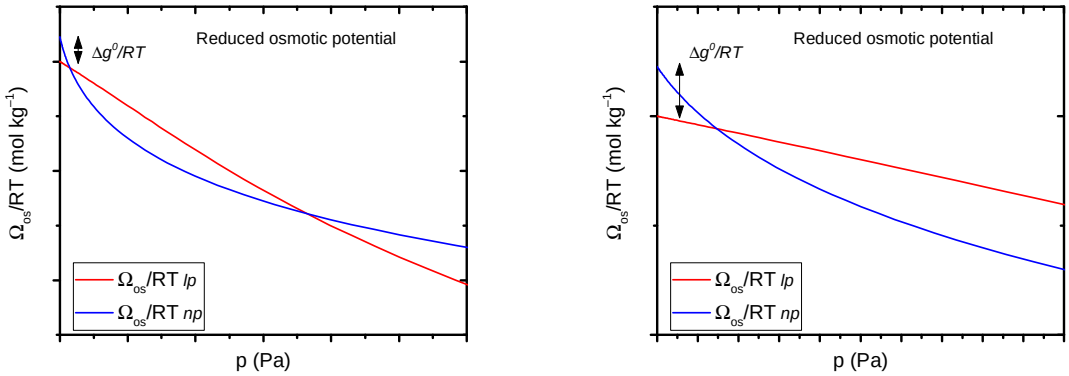

Figure 6: Schematic representation of reduced osmotic potential (Ω_{OS}/RT) vs. pressure. Ω_{OS}/RT is obtained from Ψ by applying a reduced Gibbs energy difference ($\Delta g^0/RT$) which offsets the curves. The figure on the right zooms in on the low pressure region.

Osmotic stress

Whilst finding the minimum in Gibbs energy provides us with the thermodynamically stable configuration and yields information about phase stability, it cannot account for the experimentally observed hysteresis loops in MIL-53 (Al) isotherms. A number of explanations for this behaviour has been put forward in recent literature. Neimark et al. have suggested a stress-based model, requiring the material to reach a critical stress during adsorption/desorption, upon which a phase transition occurs[18]. As the stresses (and critical stresses) are dissimilar for each phase, an asymmetry arises on the adsorption and desorption branches of the isotherm, since the phase transitions occur in reverse. Triguero et al. expanded on this by expressing the stress in terms of an energy barrier for the structural transition[51]. Introducing this barrier in Monte Carlo simulations results in the emergence of hysteretic

behaviour. Moreover, by increasing the correlation in their simulated system, the steps in the isotherms became more abrupt, as seen in experiments. The authors argue that this suggests that the collective nature of a solid prevents single unit cells from transitioning through thermal fluctuations, which would lead to more gradual steps over a wider pressure range. Instead, entire layers within the crystal will transition as a whole, triggering a cascade type effect. Whilst energy barriers are a general feature in computational studies on the hysteretic behaviour of MIL-53 [52,53], Ghysels et al. argue that, due to the solid's collective behaviour, the presence of any energy barrier would in fact prevent a structural transition from happening[15]. Instead they show, through molecular simulations, that the free energy profile can change from exhibiting the typical two minima (corresponding to *lp* and *np* phases) separated by an energy barrier to a profile with an inflection, having only one minimum. Since there are now two conditions for a phase transition, namely a lower free energy and the disappearance of the energy barrier, the transition occurs at different pressures upon adsorption or desorption.

The macroscopic nature of RALF is well suited towards incorporating the osmotic stress as proposed in ref [18], defined as:

$$\sigma_{OS} = -\left(\frac{\partial \Omega_{OS}}{\partial V}\right)_{T,\mu} \quad (35)$$

Since at constant temperature $g_{s,0}$ is a constant, we can define the reduced stress as:

$$\frac{\sigma_{OS}}{RT} = -\left(\frac{\partial \Psi}{\partial V}\right)_{T,\mu} + \frac{\sigma^0}{RT} \quad (36)$$

Here, a pre-stress, $\frac{\sigma^0}{RT}$, has been introduced to be consistent with the reasoning in ref [18]. The authors argue that the stresses on the *lp* structure at the $lp \rightarrow np$ transitions are necessarily negative due to the attractive forces of the adsorbate molecules, causing a collapse of the structure. The stress on the *lp* may eventually become positive at high pressures, when the structure approaches saturation. In contrast, the *np* structure is mainly subject to positive stresses arising from repulsive forces when the structure approaches saturation. The pre-stress may be interpreted as a pre-existing stress on the empty structures, due to, for instance, lattice strain. The derivative in equation 36 can be solved analytically through the Jacobian method [54], but for the purpose of this paper it has been solved numerically within the RALF model. The only parameters to be adjusted now are the critical stresses, σ^*. Based on experimental isotherms it is found that σ^* changes approximately linearly with temperature, so that for each transition the critical stress is defined by σ_0^* and γ:

$$\sigma^*(T) = \sigma_0^* + \gamma T \quad (37)$$

Since RALF has specifically been developed to account for volume changes in the solid, no further adjustable parameters are required to fit experimental data. This is a marked advantage over the

osmotic ensemble model as used in previous studies, which uses Langmuir based expressions, whilst assuming that the two phases are rigid[2,18,55]. It then required additional model parameters to be fitted to experimental data.

Typical stress profiles for CO_2 adsorption in both the *np* and *lp* structures of MIL-53 (Al) are shown in Figure 7. Figure 8 exemplifies how upon reaching the critical stress, a step in the isotherm is observed.

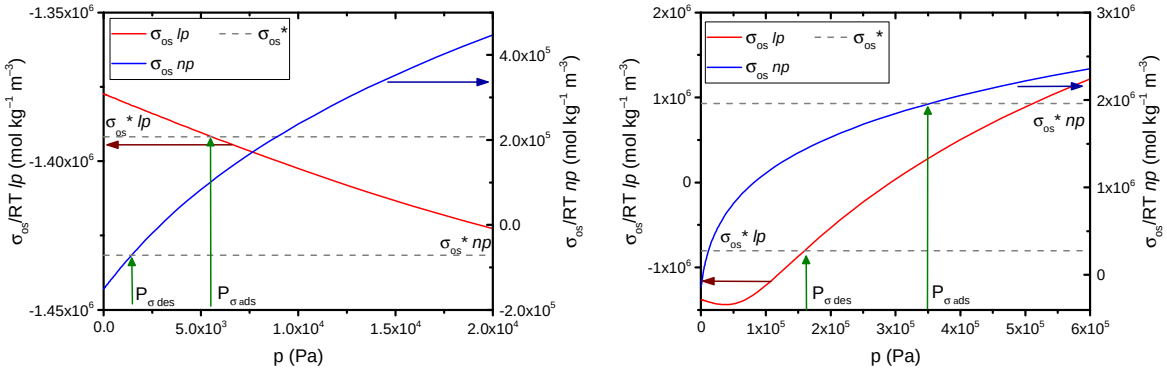

Figure 7: Stress profiles for lp and np structures at low and high pressure with critical stresses, σ^*, showing transition pressures.

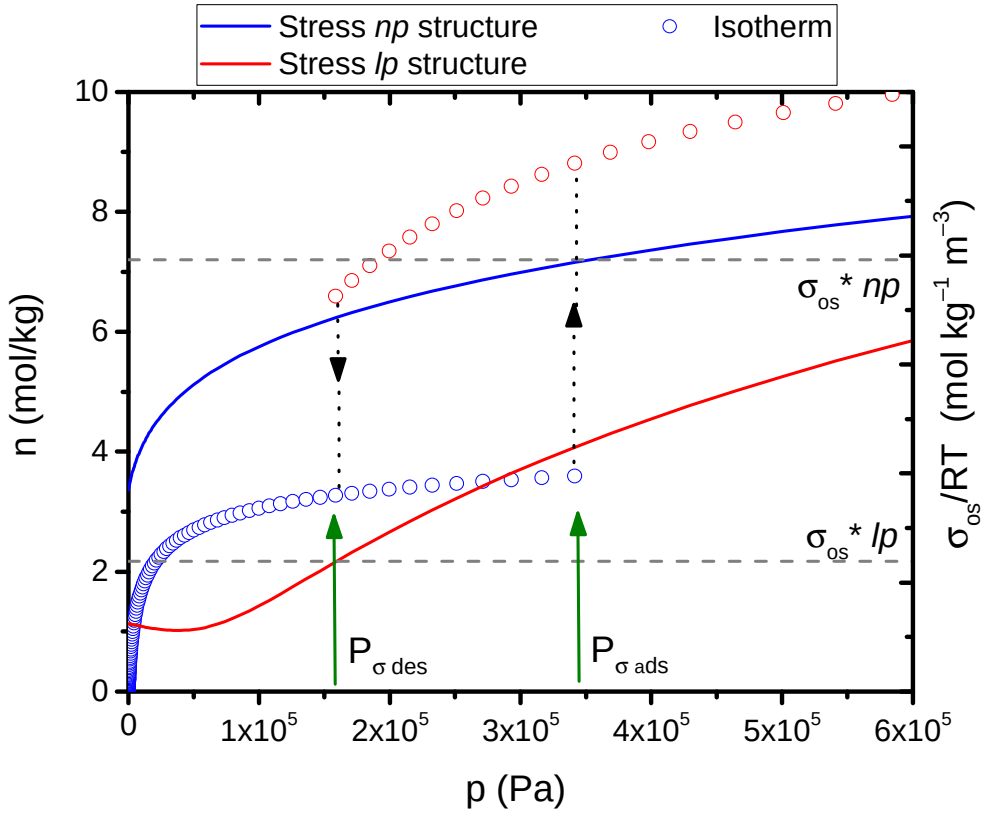

Figure 8: Effect of (critical) stresses on isotherm, resulting in hysteresis loop.

A further optimisation to the general isotherm fits can be obtained if one assumes a distribution of critical stresses, as proposed by Boutin et al.[33]. This leads to a smoothing of the transition step. Here we use a normal distribution, equation 38, with the standard deviation, *s*, as an adjustable parameter.

$$P = \frac{1}{s\sqrt{2\pi}} e^{-\left(\frac{\sigma_{OS}-\sigma^*}{s\sqrt{2}}\right)^2} \quad (38)$$

Density model of MIL-53 (Al) – two discrete structures

In order for the RALF model to describe the thermodynamic behaviour of a flexible material, an understanding of its volumetric changes on adsorption is required. It is well established that the volumetric adsorption behaviour of MIL-53 (Al) is that of a breathing material. Under vacuum and ambient temperatures it exists in its large pore structure (*lp*, unit cell volume of 1430 Å^3 under vacuum and $T = 295\ K$, as reported by Liu et al. [31]). Upon adsorbing a certain amount of molecules however, it may collapse into a narrow pore structure (*np*, unit cell volume of 887 Å^3 under vacuum, $T = 295\ K$ [31]). When increasing the partial pressure of the adsorbent further, the structure eventually

opens up again, thereby accommodating additional adsorbed molecules. The breathing effect is dependent on the nature of the guest molecules, as well as temperature and pressure[56,32,2,55,33]. The rationale for the breathing behaviour is that the *lp* structure is thermodynamically favoured under vacuum and typical temperatures for adsorption experiments. It is suggested here that the collapse to *np* structure upon adsorption happens as a result of the attractive forces between guest molecules and the solid. The re-opening to *lp* occurs due to the *np* structure becoming saturated. Further adsorption would allow a lowering of the system's Gibbs energy, but this requires reverting to the *lp* structure. This reasoning makes the breathing phenomenon and thus V_s (or ρ_s), explicitly a function of the adsorbed amount (as opposed to, for instance, the system pressure). Despite the large amount of experimental adsorption data being available in the literature, little *in situ* data is actually available on the unit cell volume for MIL-53 (Al) with varying adsorbate pressure or amount adsorbed. In this work, we will therefore explore plausible models to describe the density of MIL-53 (Al). Since volumes are additive within the lattice fluid model and to keep the number of model parameters to a minimum, we will use linear functions of the specific volume, $v_s = \frac{V_s}{m_s}$, with the amount adsorbed, although other expressions could of course be used. Based on experimental work, the *lp* is only allowed limited expansion with amount adsorbed[31,32,57], up to a unit cell volume of 1455 Å^3 (or solid density $\rho_{s,} = 950$ kg m^{-3}). Its slope with amount adsorbed is therefore fixed by using experimentally observed saturation capacities, $\frac{N^{Sat}}{m_s}$.

$v_{s,lp} = {v_{s,lp}}^0 + \frac{{v_{s,lp}}^{Sat} - {v_{s,lp}}^0}{N^{Sat}/m_s} N/m_s$	39

The *np* phase is more flexible and its slope α is assumed to be determined by the size of the guest molecules.

${v_{s,np}} = {v_{s,np}}^0 + \alpha \, {N}/{m_s}$	40

The lattice fluid model explicitly predicts this size effect from different molecules. This can be seen by considering the derivative of the close-packed lattice volume with respect to number of moles, N_k.

$\alpha \propto \frac{\partial V^*}{\partial N_k} = \frac{\partial}{\partial N_k} rNv^* = r_k^0 v_k^*$	41

It is clear that the effect is determined by pure component parameters of the adsorbate. The effect of equation 41 is easily illustrated by considering xenon and CO_2. The much bigger xenon molecule will

cause an increase in the slope α by a factor of $\frac{r_{Xe}^0 v_{Xe}^*}{r_{CO_2}^0 v_{CO_2}^*} = 1.59$ as compared to CO_2. In a multicomponent adsorbate mixture, the slope of the volume of the *np* structure with amount adsorbed simply becomes:

$$\alpha = \frac{\partial v}{\partial N} = A \sum x_k r_k^0 v_k^* \qquad (42)$$

Where *A* is a scale factor which can be is fixed by fitting pure component isotherms to experimental data. Upon phase transitions, step changes in the specific volume are assumed, as described in Figure 9. This has been found to provide the best fits to data. We have included thermal expansion data from ref. [31] to account for temperature effects on the *np* and *lp* volumes.

A gradual expansion between the *np* and *lp* structure has also been explored, but this yielded unsatisfactory results, as shown in the supplementary information. Additionally, the formation of a phase of intermediate density, labelled *int* by Bousquet et al.[49] was investigated. This phase would form on the second transition, i.e. $np \rightarrow int$, after which this *int* phase gradually expands until it reaches its maximum cell volume, 1455 Å^3. As shown in the supplementary information, this scenario also provides satisfactory results in the case of CO_2 adsorption. *In situ* diffraction data would be required for a correct representation of the volumetric behaviour of MIL-53 (Al).

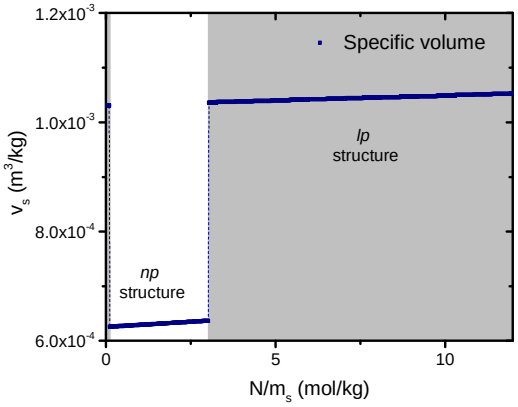

Figure 9: Schematic diagram of volumetric function with amount adsorbed.

Case study – CO_2 and CH_4 adsorption on MIL-53 (Al)

The suitability of the RALF model to predict isotherms for flexible materials is now assessed by considering two case studies: the adsorption of CO_2 and CH_4 on MIL-53 (Al). With the main characteristic parameters for the solid in place, as described in a previous section, the RALF model can now be used as a predictive model. For an accurate reproduction of experimental data however,

adjustment of the binary interaction parameter κ_{ks} and confinement parameter ξ_{kA} should be carried out. Here we use experimental data from ref. [33] to carry out this final parametrisation, with the values used in our model listed in Table 2. It is worth noting that both κ_{ks} and ξ_{kA} are temperature independent, so that once these parameters have been fixed, the solid– adsorbate system is essentially defined by two parameters. In comparison, even the simple Langmuir expression still requires three parameters to fit an equivalent system at different temperatures.

The result of the final parametrisation for CO_2 adsorption at 273 K and 298 K can be found in Figure 10. Satisfactory fits were in fact obtained between 254 K and 320 K, as can be seen for additional isotherms in the supplementary information.

Table 2: Parametrisation for CO_2 and CH_4 adsorption on MIL-53 (Al) by fitting to experimental isotherms from ref. [33]

Parameter	CO_2	CH_4
κ_{lp}	0.15	0.07
κ_{np}	–0.02	–0.10
ξ_{lp}	0.16	0.20
ξ_{np}	0.15	0.0

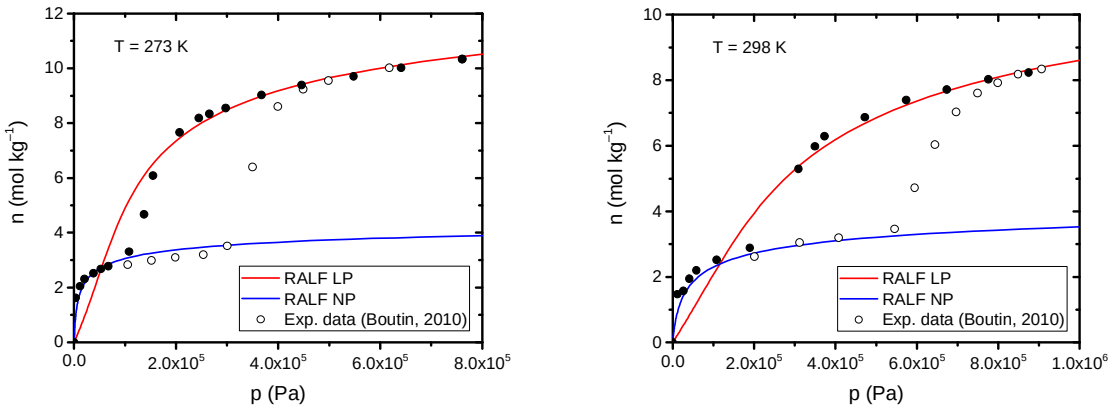

Figure 10: Fits to experimental data (ref. [33]) of the separate isotherms for lp and np structures as predicted by the RALF model.

Finally, by using the osmotic potential and osmotic stress, we can predict the true equilibrium and actual transition pressures. The resulting isotherms are shown in Figure 11. By applying a critical stress distribution, as explained in the previous sections, close fits to the experimental isotherm are obtained. CH_4 isotherms are similarly obtained and the results can be seen in Figure 12, with model

parameters also listed in Table 2. It should be noted that the predictions of the *np* section of the CH_4 isotherms are somewhat underestimated. This may be a result of the initial parameterisation of the solid energy density, P_s^*, by using simulated data on MIL-53 (Cr), since no such data was available for MIL-53 (Al). Table 3 finally provides a list of all the model parameters involved in calculating the critical stresses and distributions.

Table 3: Model parameters for calculating the critical stresses and distribution at the high pressure np ⇄ lp transition

Stress parameter	CO_2 (T = 273 K)	CH_4 (T = 213 K)
np → lp (adsorption)		
σ_0^* (mol kg^{-1} m^{-3})	$8.6 \cdot 10^6$	$1.0 \cdot 10^7$
γ (mol kg^{-1} m^{-3} K^{-1})	$-2.3 \cdot 10^4$	$-3.9 \cdot 10^4$
s	$1.0 \cdot 10^5$	$2.7 \cdot 10^5$
lp → np (desorption)		
σ_0^* (mol kg^{-1} m^{-3})	$3.0 \cdot 10^6$	$1.9 \cdot 10^6$
γ (mol kg^{-1} m^{-3} K^{-1})	$-6.6 \cdot 10^3$	$-4.2 \cdot 10^3$
s	$1.5 \cdot 10^5$	$3.2 \cdot 10^5$

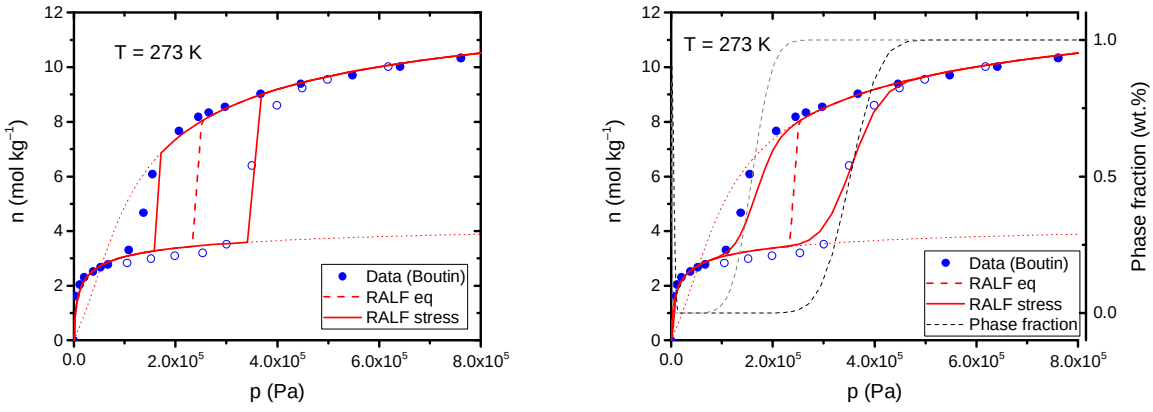

Figure 11: CO_2 isotherm at 273 K for MIL-53 (Al) as predicted by RALF and comparison with experimental data [33]. The sharp transitions from using a single critical stress (left) can be smoothed out through using a distribution of critical stresses (right). The distribution of critical stresses results in co-existence of np and lp phases over a pressure range.

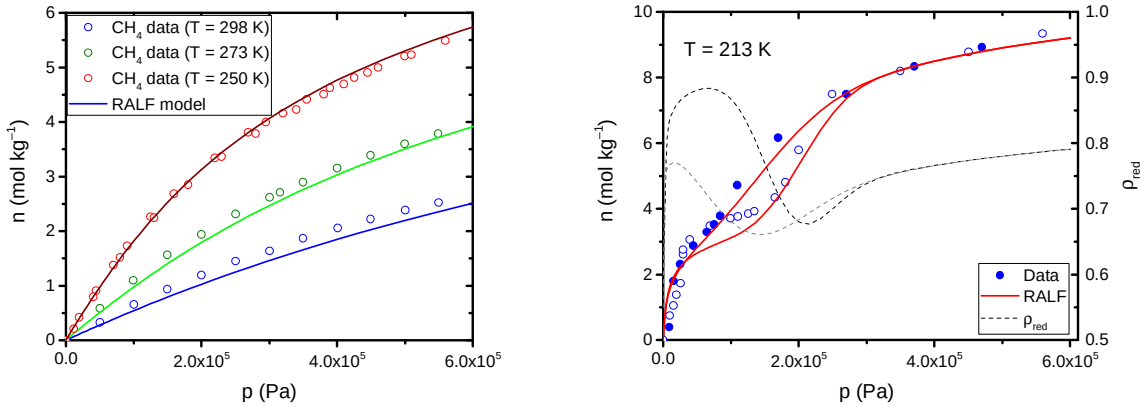

Figure 12: CH_4 isotherms at temperatures where no breathing occurs, as correctly predicted by RALF (right). CH_4 isotherm and reduced density at T = 213 K with critical stress distribution.

As discussed in the section on the system's Gibbs energy, a key model parameter is the Gibbs energy difference between the empty structures, Δg^0, (or Δh^0 and Δs^0). We have found that using $\Delta h^0 = -6.5$ kJ kg^{-1} and $\Delta s^0 = -30$ J kg^{-1} provide good agreement with experimental observations. These values would give rise to a thermally induced *lp* $\rightarrow$ *np* transition at T = 217 K, as shown in Figure 13a. This is somewhat higher than 125 – 150 K as suggested by diffraction studies by Liu et al., but a large thermal hysteresis was also observed in their work, suggesting a large window of the phases' bistability, and potential stabilising effects from energy barriers[31]. Another way of assessing the suitability of the values for Δh^0 and Δs^0, is by constructing a *P*, *T* phase stability diagram for the *np* phase as predicted by the RALF model in different atmospheres. This is shown in Figure 14a for CO_2 and CH_4. Experimental data points for CO_2 adsorption fall expectedly on either side of the phase diagram as shown in Figure 14b, due to stress induced hysteresis. Figure 13b shows that relatively small changes in Δh^0 (± 1 kJ kg^{-1}) and Δs^0 (± 2 J K^{-1} kg^{-1}) have a significant effect on the *np* phase stability. Our values for Δh^0 and Δs^0 are in reasonable agreement with those used by Boutin et al. in their Langmuir based expressions for the osmotic potentials (15 kJ kg^{-1} and 74 J K^{-1} kg^{-1}, respectively). The resulting Gibbs energy differences (e.g. 2.5 kJ kg^{-1} at 300 K) also seem to be in line with experimental work by Rodriguez[39]. Computational studies however seem to estimate much larger free energy differences between the two structures, with values ranging from –70 to –130 kJ kg^{-1} at 300 K in force field based work[37,40,58], whereas DFT studies predict energy differences of –40 to –50 kJ kg^{-1} at 0 K[36]. The discrepancies are probably partly due to oversimplifications in the RALF model. The actual Gibbs energy differences between the two structures results from a delicate balance between attraction/repulsion by the inorganic chains, dispersive forces from the organic moieties and entropic factors[36]. Nevertheless, the aim of the RALF model is not to provide molecular insight, but to accurately reproduce isotherms in order to aid in process simulations.

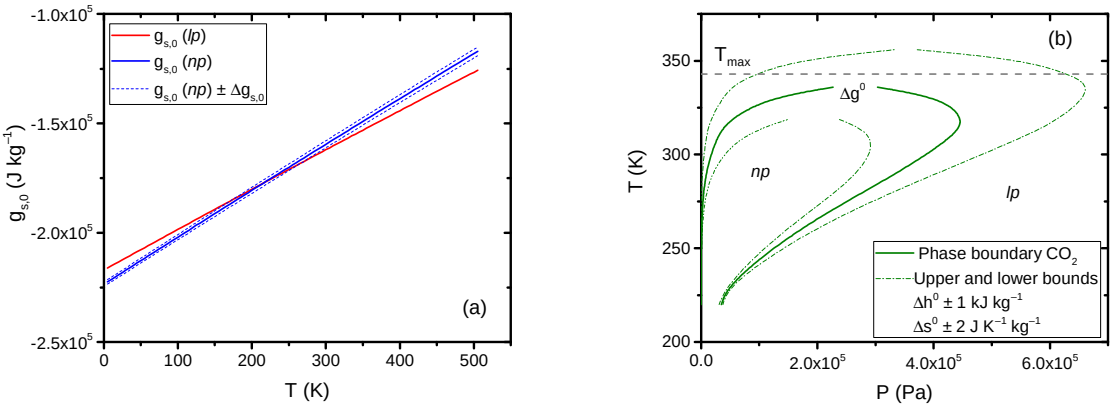

Figure 13: Gibbs energies of the empty lp and np structures, showing thermally induced transition at T = 217 K. The dashed lines correspond to maximum deviation using $\Delta h^0 = \pm 1\ kJ\ kg^{-1}$ and $\Delta s^0 = \pm 2\ J\ K^{-1} kg^{-1}$, with transition temperatures of T = 172 K and 268 K, respectively (a). The np phase stability diagram is rather sensitive to relatively small changes in Δh^0 and Δs^0 as shown in the P,T phase diagram for CO_2 (b).

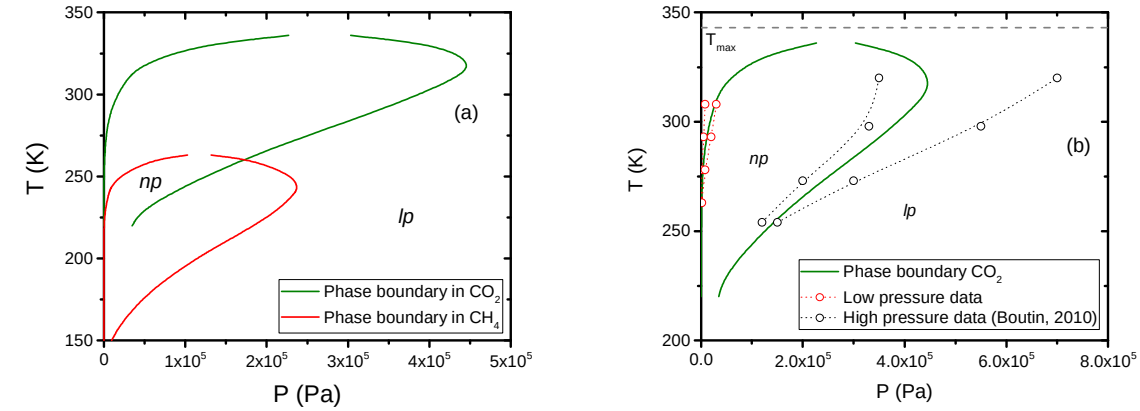

Figure 14: CO_2 and CH_4 phase stability diagrams as predicted by the RALF model (a). CO2 phase stability diagram with data points, showing predicted equilibrium transitions between experimentally observed transitions (b)[33].

Discussion

The results presented in this paper show that the RALF model, despite its simplicity, yields a surprisingly accurate representation of the breathing behaviour in MIL-53 (Al). Whereas other simplified models exist to describe this type of behaviour, such as the osmotic ensemble model proposed by Coudert et al., these rely on Langmuir expressions, which may not be appropriate for certain combinations of solids and adsorbates. Additionally, for every such combination, the Langmuir parameters and heat of adsorption will have to be determined from experiments or molecular simulations for the model to become predictive. The lattice fluid expressions used in this

study on the other hand, directly account for solid – molecule and molecule – molecule interactions, through the various characteristic parameters. This means that once the solid has been parameterised on a small number of adsorbate molecules, the model becomes predictive for any other molecules. For an improved match with experimental data, the binary interaction parameter κ_{ks} and confinement parameter ξ_{kA} can be introduced, but since these are temperature independent, one fewer parameter requires fitting as compared with using Langmuir type expressions. The model RALF also offers the flexibility of being able to accommodate any volumetric relationship, allowing for a more accurate representation of the non-rigid nature of adsorbents.

As compared to earlier incarnations of lattice fluid models[27], a distinct advantage of the RALF model is the derivation of the chemical potential of the solid. As shown in this work, phase stability is predicted directly through this thermodynamic function. The osmotic stress can also be calculated explicitly from this quantity, as long as an expression is available which describes the volumetric behaviour of the adsorbent. It has been shown that the osmotic stress allows for an accurate representation of the hysteretic behaviour in MIL-53 (Al).

One of the key modelling parameters to describe the breathing behaviour in this paper, is Δg^0(or Δh^0 and Δs^0). These values were chosen such that the empty *lp* structure is more stable than the *np* structure at room temperature, in line with experiments showing that the *lp* structure is observed under vacuum and ambient conditions[31,33]. Whilst computational studies certainly seem to agree that this is the correct interpretation for MIL-53 (Cr), recent molecular simulation studies have instead suggested that it is the *np* phase in MIL-53 (Al) that is more stable under these conditions[37,40]. Due to synthetic conditions, the *lp* phase is generally obtained, and it could be argued that it is simply stabilised through an energy barrier as previously discussed. However, this would also mean that once the material assumes the *np* phase and remains at low pressures, which would be the case during a typical desorption experiment, it should remain in its most stable *np* configuration. This seems to be in contradiction with experimental observations. For this reason, and for the purpose of showing how a relatively simple lattice fluid model can reproduce the complicated breathing behaviour of a flexible MOF, we have opted for the conventional view of the free energy relationship between *lp* and *np* phases. By adjusting Δg^0 we could easily account for the alternative free energy difference, however, which would then result in only one transition (*np* → *lp*) per adsorption/desorption cycle.

In the RALF model, ultimately, the only parameter which effects a typical breathing transition in the isotherms, is a step change in the solid density. This result is afforded by keeping all characteristic parameters for the solid constant. We have argued that the chemical coordination does not change on going from *np* to *lp* structure, leading to one set of characteristic parameters for both phases. This may be an oversimplification, as the organic linkers will show increased dispersive interaction in the *np* phase due to π interactions from the benzene rings, whilst some tilting of the metal octahedra takes

place additionally, both affecting the interaction energy[36,38]. However, these changes should be reflected in the use of separate κ_{ks} parameters for both phases. Indeed, one may argue that the values for κ_{ks} for *np* and *lp* structures are in fact too dissimilar for two related structures. However, it is evident from separation studies that the two structures have distinctly different affinities for molecules such as CO_2 and CH_4, leading to step changes in separation selectivity, and hence dissimilar κ_{ks} parameters are to be expected[4,59]. Throughout this study we have also assumed that the values for κ_{ks} and ξ_{kA} assume two constant values for each phase and are thus independent of the solid's density. This seems a reasonable assumption for MIL-53 (Al), whose volumetric behaviour seems accurately described by large step changes and small linear expansions within each structure. In materials with more subtle structural changes however, such as cation movement or minor symmetry changes, allowing for κ_{ks} to be expressed as a function of solid volume may be considered.

Conclusions

We have shown that a relatively simple model based on a lattice fluid accurately captures the breathing behaviour in MIL-53 (Al) for CO_2 and CH_4. By treating the solid phases as having different densities, but otherwise being identical, the RALF model predicts breathing transitions based on the Gibbs energy of the adsorbate – adsorbent system. This basic model, which predicts true equilibrium transitions, is based on only few parameters, most of which can be determined (and thereafter fixed) using available data from experiments or molecular simulations. Hysteresis effects can easily be incorporated by calculating the osmotic stress on the material's structure. More importantly, the RALF model is versatile and should be able to predict adsorption in a plethora of materials that undergo physical changes during this process. By changing the expressions for the solid volume or binary interaction parameter for instance, different effects on the adsorbent, which occur on the molecular level, could be described in an otherwise macroscopic model. Ultimately, RALF represents a thermodynamic model that is capable of predicting mixture behaviour in adsorbent systems without additional assumptions and may thus serve as a very helpful engineering tool in process simulation and design.

Acknowledgements

The authors would like to acknowledge funding from the Engineering and Physical Sciences Research Council, grants EP/N033329/1 (Cation controlled gating for Selective Gas Adsorption over Adaptable Zeolites) and EP/N024613/1 (Versatile Adsorption Processes for the Capture of Carbon Dioxide from Industrial Sources – FlexICCS).

Supporting information

- Additional fits to experimental CO_2 isotherms for parametrisation of binary interaction parameter κ_{jk} and confinement parameter ξ_{jA}.
- Discussion and results using alternative volumetric behaviour for the solid.
- Appendix 1: Lattice Fluid theory
- Appendix 2: Derivations of the chemical potentials

References

(1) Jeffroy, M.; Fuchs, A. H.; Boutin, A. Structural Changes in Nanoporous Solids Due to Fluid Adsorption: Thermodynamic Analysis and Monte Carlo Simulations. *Chem. Commun.* **2008**, No. 28, 3275–3277.

(2) Coudert, F.-X.; Jeffroy, M.; Fuchs, A. H.; Boutin, A.; Mellot-Draznieks, C. Thermodynamics of Guest-Induced Structural Transitions in Hybrid Organic−Inorganic Frameworks. *J. Am. Chem. Soc.* **2008**, *130*, 14294–14302.

(3) Lozinska, M. M.; Mangano, E.; Mowat, J. P. S.; Shepherd, A. M.; Howe, R. F.; Thompson, S. P.; Parker, J. E.; Brandani, S.; Wright, P. A. Understanding Carbon Dioxide Adsorption on Univalent Cation Forms of the Flexible Zeolite Rho at Conditions Relevant to Carbon Capture from Flue Gases. *J. Am. Chem. Soc.* **2012**, *134*, 17628–17642.

(4) Remy, T.; Baron, G. V.; Denayer, J. F. M. Modeling the Effect of Structural Changes during Dynamic Separation Processes on MOFs. *Langmuir* **2011**, *27*, 13064–13071.

(5) Schneemann, A.; Bon, V.; Schwedler, I.; Senkovska, I.; Kaskel, S.; Fischer, R. A. Flexible Metal–Organic Frameworks. *Chem. Soc. Rev.* **2014**, *43*, 6062–6096.

(6) Greenaway Alex G.; Shin Jiho; Cox Paul A.; Shiko Elenica; Thompson Stephen P.; Brandani Stefano; Hong Suk Bong; Wright Paul A. Structural Changes of Synthetic Paulingite (Na,H-ECR-18) upon Dehydration and CO2 Adsorption. *Z. Für Krist. - Cryst. Mater.* **2015**, *230*, 223.

(7) Lozinska, M. M.; Mangano, E.; Greenaway, A. G.; Fletcher, R.; Thompson, S. P.; Murray, C. A.; Brandani, S.; Wright, P. A. Cation Control of Molecular Sieving by Flexible Li-Containing Zeolite Rho. *J. Phys. Chem. C* **2016**, *120*, 19652–19662.

(8) Van Assche, T. R. C.; Baron, G. V.; Denayer, J. F. M. Molecular Separations with Breathing Metal–Organic Frameworks: Modelling Packed Bed Adsorbers. *Dalton Trans.* **2016**, *45*, 4416–4430.

(9) Serre C.; Bourrelly S.; Vimont A.; Ramsahye N. A.; Maurin G.; Llewellyn P. L.; Daturi M.; Filinchuk Y.; Leynaud O.; Barnes P.; et al. An Explanation for the Very Large Breathing Effect of a Metal–Organic Framework during CO2 Adsorption. *Adv. Mater.* **2007**, *19*, 2246–2251.

(10) Myers, A. L.; Monson, P. A. Physical Adsorption of Gases: The Case for Absolute Adsorption as the Basis for Thermodynamic Analysis. *Adsorption* **2014**, *20*, 591–622.

(11) Ruthven, D. M. *Principles of Adsorption and Adsorption Processes*; John Wiley & Sons, 1984.

(12) García-Pérez, E.; Serra-Crespo, P.; Hamad, S.; Kapteijn, F.; Gascon, J. Molecular Simulation of Gas Adsorption and Diffusion in a Breathing MOF Using a Rigid Force Field. *Phys. Chem. Chem. Phys.* **2014**, *16*, 16060–16066.

(13) Santander, J. E.; Tsapatsis, M.; Auerbach, S. M. Simulating Adsorptive Expansion of Zeolites: Application to Biomass-Derived Solutions in Contact with Silicalite. *Langmuir* **2013**, *29*, 4866–4876.

(14) Meza-Morales, P. J.; Gómez-Gualdrón, D. A.; Arrieta-Perez, R. R.; Hernández-Maldonado, A. J.; Snurr, R. Q.; Curet-Arana, M. C. CO2 Adsorption-Induced Structural Changes in Coordination Polymer Ligands Elucidated via Molecular Simulations and Experiments. *Dalton Trans.* **2016**, *45*, 17168–17178.

(15) Ghysels, A.; Vanduyfhuys, L.; Vandichel, M.; Waroquier, M.; Van Speybroeck, V.; Smit, B. On the Thermodynamics of Framework Breathing: A Free Energy Model for Gas Adsorption in MIL-53. *J. Phys. Chem. C* **2013**, *117*, 11540–11554.
(16) Bousquet, D.; Coudert, F.-X.; Boutin, A. Free Energy Landscapes for the Thermodynamic Understanding of Adsorption-Induced Deformations and Structural Transitions in Porous Materials. *J. Chem. Phys.* **2012**, *137*, 044118.
(17) Coudert, F.-X.; Boutin, A.; Jeffroy, M.; Mellot-Draznieks, C.; Fuchs, A. H. Thermodynamic Methods and Models to Study Flexible Metal–Organic Frameworks. *ChemPhysChem* **2011**, *12*, 247–258.
(18) Neimark, A. V.; Coudert, F.-X.; Boutin, A.; Fuchs, A. H. Stress-Based Model for the Breathing of Metal−Organic Frameworks. *J. Phys. Chem. Lett.* **2010**, *1*, 445–449.
(19) Dunne, L. J.; Manos, G. Exact Matrix Treatment of an Osmotic Ensemble Model of Adsorption and Pressure Induced Structural Transitions in Metal Organic Frameworks. *Dalton Trans.* **2016**, *45*, 4213–4217.
(20) Dunne, L. J.; Manos, G. Statistical Mechanics of Binary Mixture Adsorption in Metal–Organic Frameworks in the Osmotic Ensemble. *Philos. Trans. R. Soc. Math. Phys. Eng. Sci.* **2018**, *376*.
(21) Simon, C. M.; Braun, E.; Carraro, C.; Smit, B. Statistical Mechanical Model of Gas Adsorption in Porous Crystals with Dynamic Moieties. *Proc. Natl. Acad. Sci.* **2017**.
(22) Sanchez, I. C.; Lacombe, R. H. An Elementary Molecular Theory of Classical Fluids. Pure Fluids. *J. Phys. Chem.* **1976**, *80*, 2352–2362.
(23) Lacombe, R. H.; Sanchez, I. C. Statistical Thermodynamics of Fluid Mixtures. *J. Phys. Chem.* **1976**, *80*, 2568–2580.
(24) Sanchez, I. C.; Lacombe, R. H. Statistical Thermodynamics of Polymer Solutions. *Macromolecules* **1978**, *11*, 1145–1156.
(25) Suwanayuen, S.; Danner, R. P. A Gas Adsorption Isotherm Equation Based on Vacancy Solution Theory. *AIChE J.* **1980**, *26*, 68–76.
(26) Suwanayuen, S.; Danner, R. P. Vacancy Solution Theory of Adsorption from Gas Mixtures. *AIChE J.* **1980**, *26*, 76–83.
(27) Doghieri, F.; Sarti, G. C. Nonequilibrium Lattice Fluids: A Predictive Model for the Solubility in Glassy Polymers. *Macromolecules* **1996**, *29*, 7885–7896.
(28) Doghieri, F.; Sarti, G. C. Predicting the Low Pressure Solubility of Gases and Vapors in Glassy Polymers by the NELF Model. *J. Membr. Sci.* **1998**, *147*, 73–86.
(29) Sarti, G. C.; Doghieri, F. Predictions of the Solubility of Gases in Glassy Polymers Based on the NELF Model. *Chem. Eng. Sci.* **1998**, *53*, 3435–3447.
(30) Brandani, S. The Rigid Adsorbent Lattice Fluid Model for Pure and Mixed Gas Adsorption. *AIChE J.* **2019**, *65*, 1304–1314.
(31) Liu, Y.; Her, J.-H.; Dailly, A.; Ramirez-Cuesta, A. J.; Neumann, D. A.; Brown, C. M. Reversible Structural Transition in MIL-53 with Large Temperature Hysteresis. *J. Am. Chem. Soc.* **2008**, *130*, 11813–11818.
(32) Trung, T. K.; Trens, P.; Tanchoux, N.; Bourrelly, S.; Llewellyn, P. L.; Loera-Serna, S.; Serre, C.; Loiseau, T.; Fajula, F.; Férey, G. Hydrocarbon Adsorption in the Flexible Metal Organic Frameworks MIL-53(Al, Cr). *J. Am. Chem. Soc.* **2008**, *130*, 16926–16932.
(33) Boutin, A.; Coudert, F.-X.; Springuel-Huet, M.-A.; Neimark, A. V.; Férey, G.; Fuchs, A. H. The Behavior of Flexible MIL-53(Al) upon CH4 and CO2 Adsorption. *J. Phys. Chem. C* **2010**, *114*, 22237–22244.
(34) Bourrelly, S.; Llewellyn, P. L.; Serre, C.; Millange, F.; Loiseau, T.; Férey, G. Different Adsorption Behaviors of Methane and Carbon Dioxide in the Isotypic Nanoporous Metal Terephthalates MIL-53 and MIL-47. *J. Am. Chem. Soc.* **2005**, *127*, 13519–13521.
(35) Mishra, P.; Uppara, H. P.; Mandal, B.; Gumma, S. Adsorption and Separation of Carbon Dioxide Using MIL-53(Al) Metal-Organic Framework. *Ind. Eng. Chem. Res.* **2014**, *53*, 19747–19753.
(36) Walker Andrew M.; Civalleri Bartolomeo; Slater Ben; Mellot-Draznieks Caroline; Corà Furio; Zicovich-Wilson Claudio M.; Román-Pérez Guillermo; Soler José M.; Gale Julian D. Flexibility in a Metal–Organic Framework Material Controlled by Weak Dispersion Forces: The Bistability of MIL-53(Al). *Angew. Chem. Int. Ed.* **2010**, *49*, 7501–7503.

(37) Demuynck, R.; Rogge, S. M. J.; Vanduyfhuys, L.; Wieme, J.; Waroquier, M.; Van Speybroeck, V. Efficient Construction of Free Energy Profiles of Breathing Metal–Organic Frameworks Using Advanced Molecular Dynamics Simulations. *J. Chem. Theory Comput.* **2017**, *13*, 5861–5873.
(38) Loiseau, T.; Serre, C.; Huguenard, C.; Fink, G.; Taulelle, F.; Henry, M.; Bataille, T.; Férey, G. A Rationale for the Large Breathing of the Porous Aluminum Terephthalate (MIL-53) Upon Hydration. *Chem. – Eur. J.* **2004**, *10*, 1373–1382.
(39) Rodriguez Julien; Beurroies Isabelle; Loiseau Thierry; Denoyel Renaud; Llewellyn Philip L. The Direct Heat Measurement of Mechanical Energy Storage Metal–Organic Frameworks. *Angew. Chem. Int. Ed.* **2015**, *54*, 4626–4630.
(40) Vanduyfhuys, L.; Ghysels, A.; Rogge, S. M. J.; Demuynck, R.; Van Speybroeck, V. Semi-Analytical Mean-Field Model for Predicting Breathing in Metal–Organic Frameworks. *Mol. Simul.* **2015**, *41*, 1311–1328.
(41) Rosenbach Jr, N.; Ghoufi, A.; Déroche, I.; Llewellyn, P. L.; Devic, T.; Bourrelly, S.; Serre, C.; Férey, G.; Maurin, G. Adsorption of Light Hydrocarbons in the Flexible MIL-53(Cr) and Rigid MIL-47(V) Metal–Organic Frameworks: A Combination of Molecular Simulations and Microcalorimetry/Gravimetry Measurements. *Phys. Chem. Chem. Phys.* **2010**, *12*, 6428–6437.
(42) Cockayne, E. Thermodynamics of the Flexible Metal–Organic Framework Material MIL-53(Cr) From First-Principles. *J. Phys. Chem. C* **2017**, *121*, 4312–4317.
(43) Smith, J. M.; Van Ness, H. C.; Abbott, M. M. *Introduction to Chemical Engineering Thermodynamics*, 7th ed.; McGraw-Hill Education, 2004.
(44) Gmehling, J.; Kolbe, B.; Kleiber, M.; Rarey, J. *Chemical Thermodynamics for Process Simulation*, 1st ed.; Wiley-VCH Verlag, 2012.
(45) De Angelis, M. G.; Sarti, G. C.; Doghieri, F. NELF Model Prediction of the Infinite Dilution Gas Solubility in Glassy Polymers. *J. Membr. Sci.* **2007**, *289*, 106–122.
(46) Camacho, B. C. R.; Ribeiro, R. P. P. L.; Esteves, I. A. A. C.; Mota, J. P. B. Adsorption Equilibrium of Carbon Dioxide and Nitrogen on the MIL-53(Al) Metal Organic Framework. *Sep. Purif. Technol.* **2015**, *141*, 150–159.
(47) Ribeiro, R. P. P. L.; Camacho, B. C. R.; Lyubchyk, A.; Esteves, I. A. A. C.; Cruz, F. J. A. L.; Mota, J. P. B. Experimental and Computational Study of Ethane and Ethylene Adsorption in the MIL-53(Al) Metal Organic Framework. *Microporous Mesoporous Mater.* **2016**, *230*, 154–165.
(48) Trung, T. K.; Déroche, I.; Rivera, A.; Yang, Q.; Yot, P.; Ramsahye, N.; Vinot, S. D.; Devic, T.; Horcajada, P.; Serre, C.; et al. Hydrocarbon Adsorption in the Isostructural Metal Organic Frameworks MIL-53(Cr) and MIL-47(V). *High Surf. Area Porous Mater.* **2011**, *140*, 114–119.
(49) Bousquet, D.; Coudert, F.-X.; Fossati, A. G. J.; Neimark, A. V.; Fuchs, A. H.; Boutin, A. Adsorption Induced Transitions in Soft Porous Crystals: An Osmotic Potential Approach to Multistability and Intermediate Structures. *J. Chem. Phys.* **2013**, *138*, 174706.
(50) Kloutse, F. A.; Zacharia, R.; Cossement, D.; Chahine, R. Specific Heat Capacities of MOF-5, Cu-BTC, Fe-BTC, MOF-177 and MIL-53 (Al) over Wide Temperature Ranges: Measurements and Application of Empirical Group Contribution Method. *Microporous Mesoporous Mater.* **2015**, *217*, 1–5.
(51) Triguero, C.; Coudert, F.-X.; Boutin, A.; Fuchs, A. H.; Neimark, A. V. Mechanism of Breathing Transitions in Metal–Organic Frameworks. *J. Phys. Chem. Lett.* **2011**, *2*, 2033–2037.
(52) Beurroies Isabelle; Boulhout Mohammed; Llewellyn Philip L.; Kuchta Bogdan; Férey Gérard; Serre Christian; Denoyel Renaud. Using Pressure to Provoke the Structural Transition of Metal–Organic Frameworks. *Angew. Chem. Int. Ed.* **2010**, *49*, 7526–7529.
(53) Watanabe, S.; Sugiyama, H.; Adachi, H.; Tanaka, H.; Miyahara, M. T. Free Energy Analysis for Adsorption-Induced Lattice Transition of Flexible Coordination Framework. *J. Chem. Phys.* **2009**, *130*, 164707.
(54) Pinkerton, R. C. A Jacobian Method for the Rapid Evaluation of Thermodynamic Derivatives, without the Use of Tables. *J. Phys. Chem.* **1952**, *56*, 799–800.
(55) Boutin Anne; Springuel-Huet Marie-Anne; Nossov Andrei; Gédéon Antoine; Loiseau Thierry; Volkringer Christophe; Férey Gérard; Coudert François-Xavier; Fuchs Alain H. Breathing

Transitions in MIL-53(Al) Metal–Organic Framework Upon Xenon Adsorption. *Angew. Chem. Int. Ed.* **2009**, *48*, 8314–8317.

(56) Llewellyn, P. L.; Maurin, G.; Devic, T.; Loera-Serna, S.; Rosenbach, N.; Serre, C.; Bourrelly, S.; Horcajada, P.; Filinchuk, Y.; Férey, G. Prediction of the Conditions for Breathing of Metal Organic Framework Materials Using a Combination of X-Ray Powder Diffraction, Microcalorimetry, and Molecular Simulation. *J. Am. Chem. Soc.* **2008**, *130*, 12808–12814.

(57) Neimark, A. V.; Coudert, F.-X.; Triguero, C.; Boutin, A.; Fuchs, A. H.; Beurroies, I.; Denoyel, R. Structural Transitions in MIL-53 (Cr): View from Outside and Inside. *Langmuir* **2011**, *27*, 4734–4741.

(58) Yot, P. G.; Boudene, Z.; Macia, J.; Granier, D.; Vanduyfhuys, L.; Verstraelen, T.; Van Speybroeck, V.; Devic, T.; Serre, C.; Férey, G.; et al. Metal–Organic Frameworks as Potential Shock Absorbers: The Case of the Highly Flexible MIL-53(Al). *Chem. Commun.* **2014**, *50*, 9462–9464.

(59) Finsy, V.; Ma, L.; Alaerts, L.; De Vos, D. E.; Baron, G. V.; Denayer, J. F. M. Separation of CO2/CH4 Mixtures with the MIL-53(Al) Metal–Organic Framework. *Microporous Mesoporous Mater.* **2009**, *120*, 221–227.

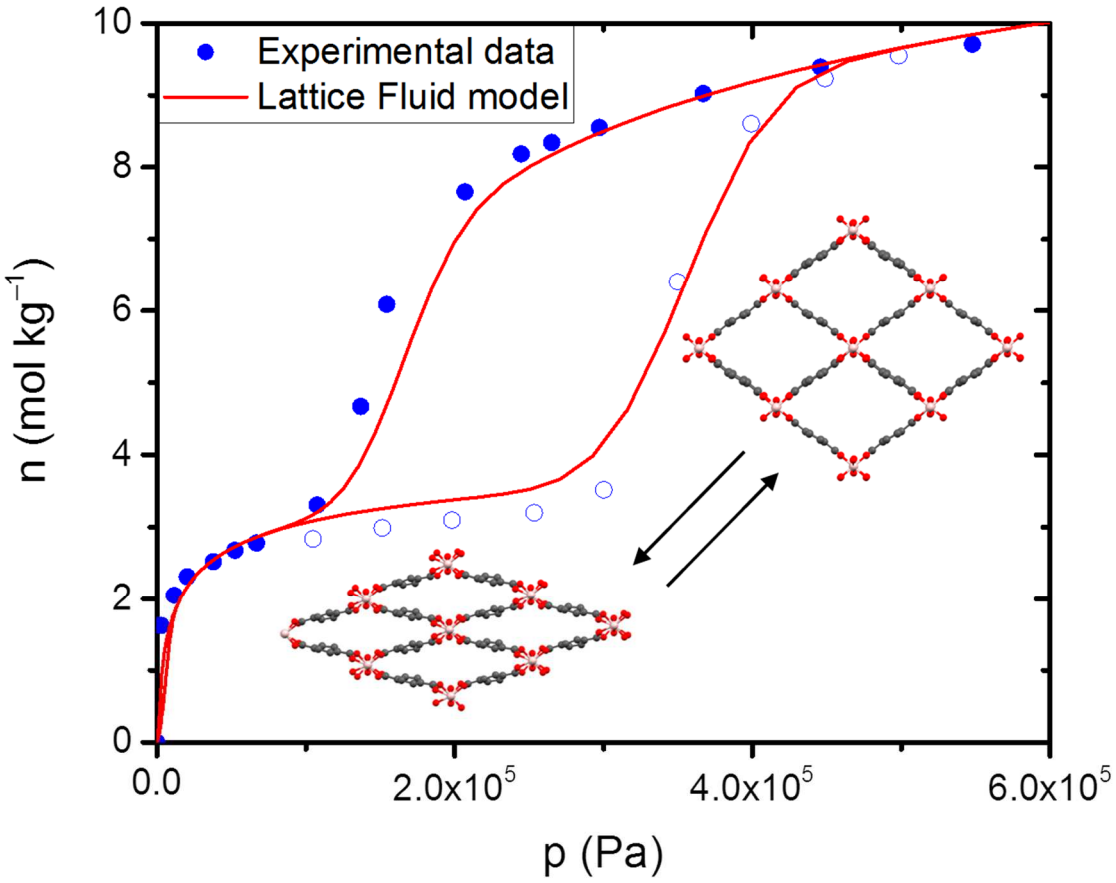

Table of Content Graphic